Multirhythmicity in an optoelectronic oscillator with large delay

Lionel Weicker,[1,2,3,*] Thomas Erneux,[1] David P. Rosin,[4] and Daniel J. Gauthier[4]
[1]*Optique Nonlinéaire Théorique, Université Libre de Bruxelles, Campus Plaine, CP 231, 1050 Bruxelles, Belgium*
[2]*Applied Physics Research Group (APHY), Vrije Universiteit Brussel, 1050 Brussels, Belgium*
[3]*OPTEL Research Group, CentraleSupélec, LMOPS (EA 4423), 2 rue Édouard Belin, 57070 Metz, France*
[4]*Department of Physics, Duke University, Durham, North Carolina 27708, USA*
(Received 6 October 2014; published 13 January 2015)

An optoelectronic oscillator exhibiting a large delay in its feedback loop is studied both experimentally and theoretically. We show that multiple square-wave oscillations may coexist for the same values of the parameters (multirhythmicity). Depending on the sign of the phase shift, these regimes admit either periods close to an integer fraction of the delay or periods close to an odd integer fraction of twice the delay. These periodic solutions emerge from successive Hopf bifurcation points and stabilize at a finite amplitude following a scenario similar to Eckhaus instability in spatially extended systems. We find quantitative agreements between experiments and numerical simulations. The linear stability of the square waves is substantiated analytically by determining the stable fixed points of a map.

DOI: 10.1103/PhysRevE.91.012910 PACS number(s): 05.45.−a, 42.65.Sf

I. INTRODUCTION

Nonlinear delay dynamics has been a particularly prolific area of research in the field of photonic devices during the last 30 years [1]. A large variety of setups exhibiting optical or electro-optical delayed feedback loops have been explored for novel applications, but also as experimental tools for delay systems in general. They have stimulated fruitful interactions with researchers working in different fields by emphasizing specific delay-induced phenomena [2–9]. Examples include different forms of oscillatory instabilities, stabilization techniques using a delayed feedback, and synchronization mechanisms for delay-coupled systems. Most of the current lasers used in applications are semiconductor lasers (SLs), which are highly sensitive to optical feedback [10]. Here, the light coming from the laser is reflected back to the laser after a substantial delay. Another popular delay system is an optoelectronic oscillator (OEO) [11,12] that consists of a laser injecting its light into an optoelectronic loop. For OEOs, the feedback exhibits a large delay because of a long optical fiber line in the OEO closed-loop configuration. An OEO is capable of generating, within the same optoelectronic cavity, either an ultralow-jitter single-tone microwave oscillation, as used in radar applications [13], or a broadband chaotic carrier typically intended for physical data encryption in high bit rate optical communications [14,15]. The OEO is a particularly attractive system because it allows quantitative comparisons between experiments and theory [16–18].

For systems exhibiting a Hopf bifurcation in the absence of delay, a feedback with a large delay may lead to the coexistence of stable periodic solutions in the vicinity of the first Hopf bifurcation point. This multirhythmicity was predicted theoretically using a Hopf normal-form equation with a delayed feedback [19], where the bifurcation scenario is similar to Eckhaus instability in spatially extended systems [20]. The bandpass OEO without its optical fiber line admits a Hopf bifurcation. In this paper, we investigate the stabilization of nearby Hopf bifurcation branches in this regime.

Here, we conduct a systematic experimental and numerical study of an OEO exhibiting a large delay. We show that an OEO admits coexisting stable periodic square waves. Depending on the feedback phase, they are characterized by frequencies close to either $(1+2n)/(2\tau_D)$ $(n=0,1,2,\ldots)$ or n/τ_D $(n=1,2,\ldots)$, where τ_D is the delay of the feedback loop. In order to induce these periodic solutions, we inject a periodic electrical signal into the oscillator during the initialization phase of the experiment and then observe the resulting dynamics after the injected signal is removed. In the simulations, we choose different initial periodic functions in order to determine different periodic solutions.

Periodic regimes of an OEO showing frequencies that are multiples of $1/\tau_D$ were found in the past. In Refs. [21,22], the authors progressively increased the delay and investigated the sequential jump to stable oscillations of frequency $(2n+1)/(2\tau_D)$ $(n=0,1,\ldots)$. In Refs. [23,24], the authors found numerically periodic solutions of frequency close to n/τ_D. In this paper, we demonstrate the multirhythmicity phenomenon by exciting square waves with a specific frequency (specific n). Furthermore, we relate these periodic solutions to nearby Hopf bifurcation points, a prerequisite for an Eckhaus bifurcation scenario.

The experimental setup of an OEO is sketched in Fig. 1. A semiconductor laser beam is injected into a Mach-Zehnder intensity modulator (MZM). The MZM induces a nonlinear function of the applied voltage. The modulated light passes through an optical fiber, which is used as a delay line, and is injected into an inverting photodetector, which converts the signal into the electrical domain. The voltage emitted from the photodectector passes through a bandpass filter and then through a power splitter. Half of the voltage, denoted by V, is amplified by an inverting modulator driver (MD). This electric signal is then reinjected inside the MZM via its radio frequency input port to close the feedback loop. The voltage coming out of the other port of the power splitter is used to measure the dynamical variable V with a high-speed oscilloscope. The device used has an 8 GHz analog bandwidth and a 40 GS/s

*lweicker@ulb.ac.be

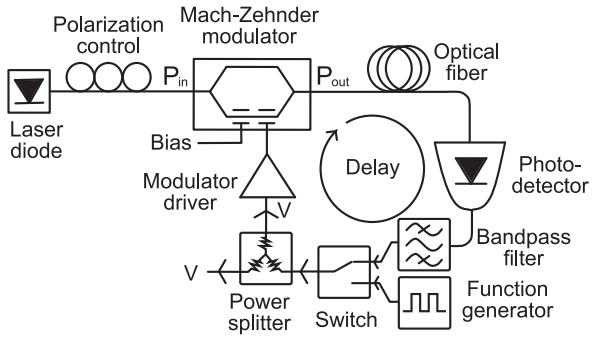

FIG. 1. Schematic of the experimental setup of an optoelectronic oscillator.

sampling rate. In our experiments, the delay of the feedback loop is fixed at $\tau_D = 22$ ns. The system described is the same as in Refs. [22,23,25] except that a pattern generator has been included to perturb the dynamics of the system. An electrical switch is used to isolate this pattern generator from the rest of the system. The switch also allows a controllable electrical signal to be combined with V at the input of the MD.

Mathematically, we consider the evolution equations formulated in Refs. [15,23] with time measured in units of the delay. They are given by [26]

$$\varepsilon \frac{dx}{ds} = -x - \delta y + \beta[\cos^2\{m + \tanh[x(s-1)]\} - \cos^2(m)], \tag{1}$$

$$\frac{dy}{ds} = x, \tag{2}$$

where $s \equiv t/\tau_D$ and x is the normalized voltage of the electrical signal in the OEO. The feedback amplitude β and the phase shift m are two control parameters. Here, $\varepsilon \simeq (\tau_D \omega_+)^{-1} = 0.0157$ and $\delta \simeq \tau_D \omega_- = 0.2042$ [26] are dimensionless time constants fixed by the low and high cutoff frequencies of the bandpass filter denoted by ω_- and ω_+, respectively. Equations (1) and (2) are the same equations studied in Ref. [25] except for the hyperbolic tangent function in Eq. (1) that accounts for the amplifier saturation.

Equations (1) and (2) admit a single steady state $(x,y) = (0,0)$ and its linear stability has been analyzed in detail in Refs. [21,25]. Of particular interest are the primary Hopf bifurcation points, which can be classified into two different families. In the limit $\delta \to 0$ and $\varepsilon \to 0$, the critical feedback amplitudes and the Hopf bifurcation frequencies approach the limits [27]

$$m > 0: \ \beta_n = 1/\sin(2m), \quad \text{and} \quad \omega_n = (1+2n)\pi \ \ (n = 0,1,2,\ldots), \tag{3}$$

$$m < 0: \ \beta_n = -1/\sin(2m), \ \omega_0 = \sqrt{\delta}, \quad \text{and} \quad \omega_n = 2n\pi \ \ (n = 1,2,\ldots). \tag{4}$$

If $m > 0$, the frequencies are odd multiples of π, meaning that the successive Hopf bifurcations lead to $2/(1+2n)$-periodic solutions [$2\tau_D/(1+2n)$-periodic solutions in physical time]. If $m < 0$ and $n = 1,2,\ldots$, the frequencies are even multiples of π and the successive Hopf bifurcations lead to $1/n$-periodic solutions (τ_D/n-periodic solutions in physical time). In addition, there exists for $m < 0$ a Hopf bifurcation characterized by the low frequency $\omega_0 = \sqrt{\delta} \ll 1$. It leads to oscillations with a large period compared to 1 (large period compared to τ_D in physical time).

The organization of the paper is as follows. In Sec. II, we describe the experimental observations and numerical simulations for the two families of Hopf bifurcations. In Sec. III, we propose a partial stability analysis of the plateaus by associating their mean values to stable fixed points of a map. Finally, we discuss our main results in Sec. IV.

II. EXPERIMENTS AND SIMULATIONS

From the linear stability analysis of the zero solution discussed above, we find that there exist two families of Hopf bifurcations depending on the sign of m. For each case, we describe our experimental observations and compare them to numerical simulations of Eqs. (1) and (2).

A. Case $m > 0$

If $m > 0$, oscillations of period close to $2\tau_D$ (corresponding to a frequency of 22.7 MHz) are observed experimentally [see Fig. 2(a)]. In order to find harmonic oscillations, we excite the system with signals at different frequencies. To this end, the pattern generator injects different periodic signals into the OEO loop for a few seconds. Figure 2(b) shows square-wave oscillations of period close to $2\tau_D/5$ obtained by injecting a square-wave signal of frequency 114 MHz. Similarly, by exciting the OEO with sine-wave signals of frequency 159 MHz and of frequency 205 MHz, we obtain $2\tau_D/7$- and $2\tau_D/9$-periodic oscillations, respectively [Figs. 2(c) and 2(d), respectively]. $2\tau_D/3$-periodic oscillations are also observed

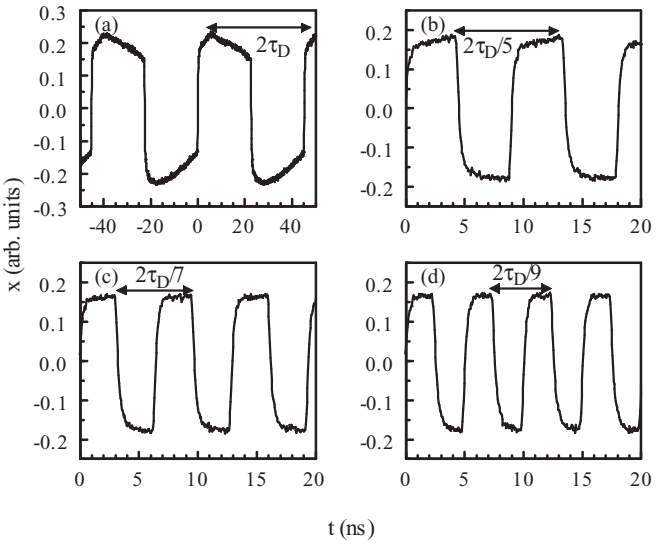

FIG. 2. Experimental time series obtained after injecting different periodic signals into the OEO loop for a few seconds and after the injected signal is removed. The measured values of the parameters are $m = 0.665$, $\beta = 1.94$, and $\tau_D = 22$ ns.

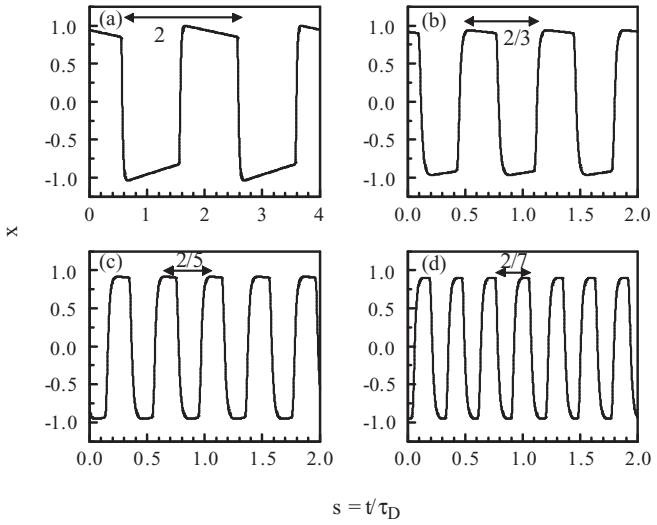

FIG. 3. Numerical time series obtained from Eqs. (1) and (2). (a) Oscillations of period close to 2 with $x(s) = \cos(\pi s)$ and $y(s) = 0$ $(-1 < s < 0)$; (b) oscillations of period close to 2/3 with $x(s) = \cos(3\pi s)$ and $y(s) = 0$ $(-1 < s < 0)$; (c) oscillations of period close to 2/5 with $x(s) = \cos(5\pi s)$ and $y(s) = 0$ $(-1 < s < 0)$; (d) oscillations of period close to 2/7 with $x(s) = \cos(7\pi s)$ and $y(s) = 0$ $(-1 < s < 0)$. The values of the control parameters are the same as in Fig. 2: $m = 0.665$ and $\beta = 1.94$.

but are not shown for clarity. The observation of stable oscillations characterized by higher frequencies ($n > 4$) is not possible because of the bandwidth limitation of the pattern generator.

We next integrate numerically Eqs. (1) and (2) using the same values of the parameters as for the experiments. Figure 3 shows four different time series obtained using different initial functions described in the caption. We note that the shape and the period of the oscillations are in good agreement with the experimental observations. The plateaus of the square wave are slightly increasing or decreasing in time, which is an effect of the small parameters ε and δ. If we decrease their values, the plateaus become flatter. Another point raised by the numerical simulations and by the experimental observations is that the mean values of the plateaus are roughly the same for the main and harmonic periodic solutions. From Fig. 3(d), we evaluate theses values as

$$x_{\max} \simeq 0.9 \quad \text{and} \quad x_{\min} \simeq -0.95. \tag{5}$$

2/9-periodic oscillations are also found numerically but they are unstable for long times. They are stable if we slightly decrease ε. A smaller ε leads to sharper transition layers that contribute to the overall stability of the square wave. The discrepancy between the experimental and numerical solutions for the 2/9-periodic regimes could be a result of the model slightly overestimating the effect of the amplifier saturation (value of d) which contributes to smoothen the transition layers.

We also examine the effect of changing m. Figure 4(a) shows the first Hopf bifurcation lines in the (m,β) parameter plane. There is a stable steady state if $\beta < 1$. Increasing β leads to a critical point $\beta_{H1} > 1$ where oscillations of period 2

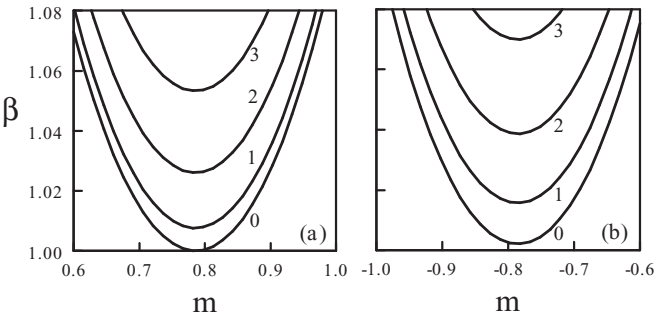

FIG. 4. Hopf bifurcation lines in the (m,β) parameter plane. (a) corresponds to the case m positive and (b) to the case m negative. They have been determined numerically from the exact conditions with $\varepsilon = 0.0157$ and $\delta = 0.2042$. The numbers in the figures indicate the value of n corresponding to a specific frequency defined in (3) and (4). All curves are nearly parabolic with a minimum at $m = \pm\pi/4$. If $\varepsilon \to 0$ and $\delta \to 0$, all curves moves to a unique parabola with minimum located at $(m,\beta) = (\pm\pi/4, 1)$.

appear. The minimal value of β_{H1} is obtained if $m = \pi/4$. By progressively increasing β from β_{H1}, we may generate stable higher-order harmonic oscillations that become more robust with respect to small perturbations.

B. Case $m < 0$

If $m < 0$, in the experiment, we observe stable square-wave oscillations of period close to τ_D/n. Figure 5(b), 5(c), and 5(d)

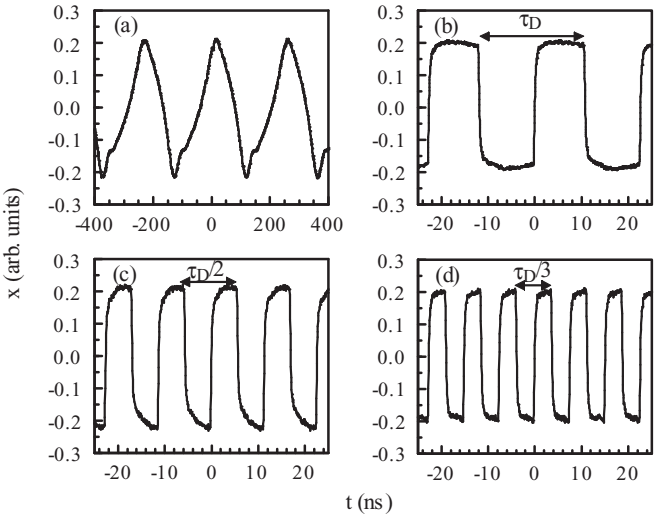

FIG. 5. Experimental time series obtained after injecting different periodic signals into the OEO loop for a few seconds and after the injected signal is removed. (a) Low-frequency oscillations of period close to $12\tau_D$ obtained by injecting a sine-wave signal of frequency 5 MHz; (b) oscillations of period close to τ_D obtained by injecting a sine-wave signal of frequency 45.5 MHz; (c) oscillations of period close to $\tau_D/2$ obtained by injecting a sine-wave signal of frequency 90.9 MHz; (d) oscillations of period close to $\tau_D/3$ obtained by injecting a sine-wave signal of frequency 136 MHz. The value of the delay is $\tau_D = 22$ ns. The measured values of the control parameters are $m = -0.845$ and $\beta = 1.94$ for (a) and (b) and $m = -0.785$ and $\beta = 2.2$ for (c) and (d).

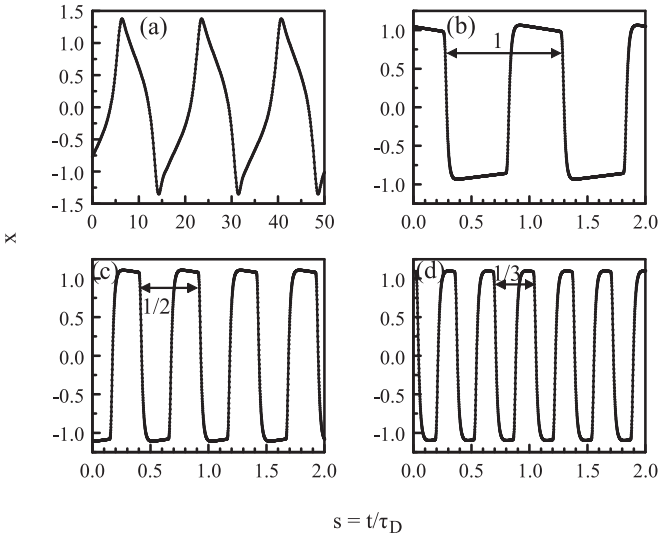

FIG. 6. Numerical time series obtained from Eqs. (1) and (2). (a) Slowly varying solutions obtained with $x(s) = \cos(0.5\pi s)$ and $y(s) = 0$ $(-1 < s < 0)$; (b) oscillations of period close to 1 with $x(s) = \cos(2\pi s)$ and $y(s) = 0$ $(-1 < s < 0)$; (c) oscillations of period close to 1/2 obtained with $x(s) = \cos(4\pi s)$ and $y(s) = 0$ $(-1 < s < 0)$; (d) oscillations of period close to 1/3 with $x(s) = \cos(6\pi s)$ and $y(s) = 0$ $(-1 < s < 0)$. The values of the control parameters are the same as in Fig. 5: $m = -0.845$ and $\beta = 1.94$ for (a) and (b) and $m = -0.785$ and $\beta = 2.2$ for (c) and (d).

show oscillations of period close to τ_D, $\tau_D/2$, and $\tau_D/3$, respectively. They are obtained by exciting the OEO with periodic signals of different frequencies, as described in the caption. Oscillations of period close to $\tau_D/4$ are also observed. Moreover, we find stable slowly varying oscillations [see Fig. 5(a)], in agreement with our previous stability analysis that predicts a Hopf bifurcation for $m < 0$ with a low frequency. As for the case $m > 0$, we do not find higher-order harmonic oscillations because of the bandwidth limitation of the pattern generator preventing us from initializing the system with frequencies above a certain threshold.

Integrating Eqs. (1) and (2) using different initial functions leads to similar time-periodic regimes. The slowly varying oscillations are shown in Fig. 6(a) and exhibit a period close to $T = 17.2$. With the Hopf bifurcation frequency ω_0 given in (4), we compute $T_0 = 2\pi/\omega_0 \simeq 14$, which is of the same order of magnitude as T. Figures 6(b)–6(d) show oscillations of period close to 1, 1/2, and 1/3, respectively.

We investigate numerically the effect of changing $m < 0$. The first Hopf bifurcation lines are shown in Fig. 4(b). In contrast to the case $m > 0$ where the square wave remains symmetric (same plateau lengths), here the shape of the square wave depends on m. If $m = -\pi/4$, we observe symmetric square-wave oscillations with a period close to τ_D/n. However, if $m + \pi/4 \neq 0$, the square wave becomes asymmetric with different duty lengths for each plateau. The total period remains constant. As for the case $m > 0$, the square-wave oscillations become more robust if β increases. The same properties are observed experimentally. Figures 6(b)–6(d) are obtained using slightly different values of the parameters m and β. From Figs. 6(c) and 6(d), we find that the mean values of the plateaus are identical for the two periodic regimes and are given by

$$x_{\max} \simeq 1.1 \quad \text{and} \quad x_{\min} \simeq -1.1. \tag{6}$$

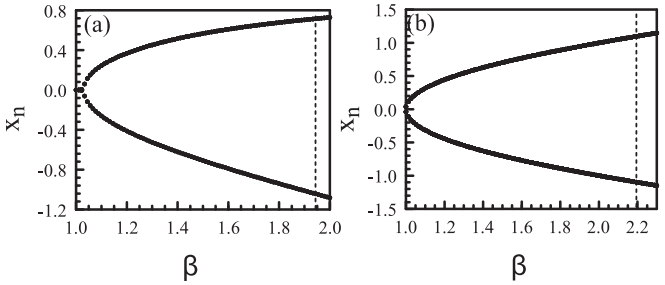

FIG. 7. Stable fixed points of Eq. (7). (a) $m = 0.665$. The diagram shows branches of a period-2 fixed point. The dashed line corresponds to the experimental and numerical value of β. (b) $m = -0.785$. The diagram shows two branches of period-1 fixed points. The dashed line corresponds to the experimental and numerical value of β.

III. LINEAR STABILITY OF THE PLATEAUS

In the limit $\delta \to 0$ and $\varepsilon \to 0$, Eqs. (1) and (2) reduce to a single equation for a map given by

$$x_{n+1} = \beta\{\cos^2[m + \tanh(x_n)] - \cos^2(m)\}. \tag{7}$$

Here, we demonstrate that the plateaus of the square waves can be partially understood by considering the stable fixed points of this map. For the case $m > 0$, there is a Hopf bifurcation at $\beta_c = 1/\sin(2m)$ to a stable period-2 fixed point [see Fig. 7(a)]. For the values of m and β used in our experiments and simulations, the diagram in Fig. 7(a) indicates

$$x_{\max} = 0.72 \quad \text{and} \quad x_{\min} = -1.04, \tag{8}$$

which agree qualitatively with the values (5) estimated from the numerical simulations.

For the case $m < 0$, Eq. (7) admits two stable period-1 fixed points that appear at $\beta_c = -1/\sin(2m)[x_n > 0$ and $x_n < 0$—see Fig. 7(b)]. For the values of the parameters used in our experiments and simulations [Figs. 5(c) and 5(d) and for Figs. 6(c) and 6(d)], the diagram in Fig. 7(b) indicates

$$x_{\max} = 1.10 \quad \text{and} \quad x_{\min} - 1.10, \tag{9}$$

which agree quantitatively with the values (6) obtained from the numerical simulations.

IV. DISCUSSION

Symmetric and asymmetric square-wave oscillations have been found previously [16,18,23,28] and were related to the first Hopf bifurcation of a basic steady state. Here, we concentrate on the next primary Hopf bifurcations and show that they quickly stabilize above critical amplitudes. This is the bifurcation scenario related to the Eckhaus instability known to exist in spatially extended systems. The Eckhaus instability has been predicted to occur in a simple model equation in the limit of large delays [19]. The idea is based on the observation that all Hopf bifurcation points

move to a critical value in the limit of large delay (in our case, $\varepsilon \to 0$ and $\delta \to 0$). We may then apply the method of multiple time scales and formulate a partial differential equation for a small amplitude solution. In Ref. [19], a single variable complex Ginzburg-Landau equation was derived for which the stability of the different periodic solutions can be demonstrated analytically. The mechanism responsible for the stabilization of each branch of the periodic solutions is called the Eckhaus instability. Assuming $\beta - 1 = O(\varepsilon^2)$ and $\delta = O(\varepsilon^2)$, we have found that two coupled partial differential equations can be derived from Eqs. (1) and (2). By contrast to the case studied in Ref. [19], these equations cannot be solved analytically. However, their similitude to the Ginzburg-Landau equation suggests that distinct stable periodic solutions may coexist through the same Eckhaus scenario. In this paper, we demonstrated both experimentally and numerically that this coexistence of square waves with distinct periods is possible. Those regimes have already been referenced in previous studies of OEOs but not as coexisting solutions. They were obtained as sequential jumps when varying either the delay [21,22] or the low-frequency cutoff [23,24]. Here, we showed how to obtain these regimes systematically in an experiment without varying any parameters of the OEO system. A remarkable property of our OEO is the possibility to compare quantitatively experimental observations and numerical simulations. It motivates asymptotic studies of the OEO equations based on the large delay limit [28].

We believe that this multirhythmicity of square waves resulting from nearby Hopf bifurcations is generic to a large class of delay systems exhibiting a large delay. Recently, we studied a semiconductor laser subject to polarization-rotated feedback [29] and found this coexistence of harmonic periodic regimes both experimentally and numerically. The laser rate equations are completely different from the dynamical equations for an OEO and are mathematically more complex to analyze. The common property is the presence of nearby Hopf bifurcation points leading to square waves with periods that are close to $2\tau_D/(2n+1)$, where $n = 0,1,2,\ldots$.

ACKNOWLEDGMENTS

L.W. acknowledges the Belgian F.R.I.A., the Conseil Régional de Lorraine, the Agence Nationale de la Recherche (ANR) TINO project (ANR-12-JS03-005) and external funds from the F.N.R.S. T.E. acknowledges the support of the F.N.R.S. This work also benefited from the support of the Belgian Science Policy Office under Grant No IAP-7/35 "photonics@be." D.P.R. and D.J.G. gratefully acknowledge the financial support by the U.S. Army Research Office, Grant No. W911NF-12-1-0099.

[1] T. Erneux and P. Glorieux, *Laser Dynamics* (Cambridge University Press, Cambridge, UK, 2010).
[2] T. Erneux, *Applied Delay Differential Equations* (Springer, New York, 2009).
[3] A. Balachandran, T. Kamár-Nagy, D. Gilsinn, and E. David, *Delay Differential Equations, Recent Advances and New Directions* (Springer, New York, 2009).
[4] G. Stepan, Philos. Trans. R. Soc., A **367**, 1059 (2009).
[5] F. Atay, *Complex Time-Delay Systems* (Springer, New York, 2010).
[6] W. Just, A. Pelster, M. Schanz, and E. Schöll, Philos. Trans. R. Soc., A **368**, 303 (2010).
[7] T. Kalmár-Nagy, N. Olgac, and G. Stépán, J. Vib. Control **16**, 941 (2010).
[8] M. Lakshmanan and D. Senthilkumar, *Dynamics of Nonlinear Time-Delay Systems* (Springer, New York, 2011).
[9] H. Smith, *An Introduction to Delay Differential Equations with Applications to the Life Sciences* (Springer, New York, 2011).
[10] M. C. Soriano, J. García-Ojalvo, C. R. Mirasso, and I. Fischer, Rev. Mod. Phys. **85**, 421 (2013).
[11] L. Larger, Philos. Trans. R. Soc., A **371**, 20120464 (2013).
[12] P. Devgan, ISRN Electron. **2013**, 401969.
[13] Y. K. Chembo, A. Hmima, P.-A. Lacourt, L. Larger, and J. M. Dudley, J. Lightwave Technol. **27**, 5160 (2009).
[14] N. Gastaud, S. Poinsot, L. Larger, J. Merolla, M. Hanna, J. Goedgebuer, and F. Malassenet, Electron. Lett. **40**, 898 (2004).
[15] K. E. Callan, L. Illing, Z. Gao, D. J. Gauthier, and E. Schöll, Phys. Rev. Lett. **104**, 113901 (2010).
[16] M. Peil, M. Jacquot, Y. K. Chembo, L. Larger, and T. Erneux, Phys. Rev. E **79**, 026208 (2009).
[17] E. C. Levy, M. Horowitz, and C. R. Menyuk, J. Opt. Soc. Am. B **26**, 148 (2009).
[18] L. Weicker, T. Erneux, O. d'Huys, J. Danckaert, M. Jacquot, Y. Chembo, and L. Larger, Phys. Rev. E **86**, 055201 (2012).
[19] M. Wolfrum and S. Yanchuk, Phys. Rev. Lett. **96**, 220201 (2006).
[20] L. S. Tuckerman and D. Barkley, Physica D: Nonlinear Phenom. **46**, 57 (1990).
[21] L. Illing and D. J. Gauthier, Physica D: Nonlinear Phenom. **210**, 180 (2005).
[22] L. Illing and D. J. Gauthier, Chaos **16**, 033119 (2006).
[23] D. P. Rosin, K. E. Callan, D. J. Gauthier, and E. Schöll, Europhys. Lett. **96**, 34001 (2011).
[24] D. Rosin, Master's thesis, Technische Universität Berlin, 2011.
[25] Y. C. Kouomou, P. Colet, L. Larger, and N. Gastaud, Phys. Rev. Lett. **95**, 203903 (2005).
[26] From Eqs. (1) and (2) in Ref. [15], we obtain our Eqs. (1) and (2) with $\varepsilon = (T\Delta)^{-1} = [T(\omega_+ - \omega_-)]^{-1}$, and $\delta = T\omega_0^2/\Delta = T(\omega_+\omega_-)/(\omega_+ - \omega_-)$ and $\beta = \gamma$. T is the delay of the feedback loop, and ω_- and ω_+ represent the low- and high-frequency cutoffs of the bandpass filter, respectively. Since $\omega_+ \gg \omega_-$, $\varepsilon \simeq (T\omega_+)^{-1}$ and $\delta \simeq T\omega_-$.
[27] From Eqs. (4) and (5) in Ref. [25], introduce $\omega \to \omega R, \delta \to \varepsilon R$, $\varepsilon \to 1/R$. The new parameters ε and δ are small and their values are given in Sec. I.
[28] L. Weicker, T. Erneux, O. D'Huys, J. Danckaert, M. Jacquot, Y. Chembo, and L. Larger, Philos. Trans. R. Soc., A **371**, 20120459 (2013).
[29] G. Friart, L. Weicker, J. Danckaert, and T. Erneux, Opt. Express **22**, 6905 (2014).